Modulation of Cell Adhesion Complexes by Surface Protein Patterns

Devrim Pesen* and David B. Haviland

Department of Applied Physics, Royal Institute of Technology, KTH, AlbaNova, Stockholm, Sweden

ABSTRACT Cell adhesion is an important process in several biological phenomena. To investigate the formation and organization of focal adhesions, we developed a patterning approach based on electron beam lithography. Nanodots (radius <1230 nm) and nanorings (inner radius <320 nm) of fibronectin (FN) were patterned on a K-Casein background. Intracellular vinculin immunofluorescence mirrored the FN nanopatterns. Atomic force microscopy showed that FN nanodots and nanorings organize the immediate cytoskeleton into straight fibrils and diverging fibril bundles, respectively. Our results suggest that a minimum of ~40 FN molecules is required for a cell to form a focal adhesion.

KEYWORDS: cell adhesion • fibronectin • atomic force microscopy • electron beam lithography

Cell adhesion is an important process in several biological phenomena such as embryonic development, angiogenesis, and metastasis. Adhesion to surfaces is mediated by proteins and complexes with sizes on the order of 10 nm to 10 μm. Focal adhesions (FAs) are comprised of an extracellular matrix protein [e.g., fibronectin (FN), laminin], a transmembrane protein (integrins) and intracellular proteins (e.g., actin, vinculin). They function as crucial outside-to-inside signaling ports and help cells function properly (1). The nanometer- and micrometer-scale organization of surface proteins is expected to play a crucial role in adhesion complex formation and function. Cell adhesion and cellular organization have been widely studied as a function of the available adhesive area and shape using micrometer-scale patterns (2, 3). However, the influence of differential organization of surface proteins at the nanometer scale has not been explored because of a lack of flexible, high-resolution nanoscale patterning techniques for biofunctional surfaces. The methods presented here demonstrate how an understanding of adhesion complex formation can greatly benefit from surfaces with custom-tailored nanometer-scale patterns.

Surface patterning can be realized through various approaches such as microcontact printing, nanografting, self-assembly, dip-pen lithography, and electron beam lithography (EBL) (4–6). Microcontact printing is an example of a parallel method, well suited for high-throughput production but limited in resolution and pattern geometry. Parallel methods require mask production, which can be time-consuming in research and development. Direct writing methods, on the other hand, are serial, with limited throughputs, but have the ability to freely change the pattern geometry. Among direct surface patterning tools for arbitrary pattern generation, EBL is one of the fastest, with a resolution down to a few nanometers due to a tightly focused electron beam (diameter ~2 nm). EBL can be used to pattern from a few nanometers to millimeters, covering the range of length scales that are important for cell biological applications. EBL has been utilized for surface patterning of proteins, including cell-adhesion-promoting types (7–11).

Surface patterns at the nanometer scale are often limited by either the fabrication speed, pattern flexibility, or biofunctionality of the resulting pattern at the cellular level (12, 13). EBL can effectively overcome these limitations and realize biofunctional patterns, where the fundamental pattern unit is a biofunctional nanodot (14). EBL also offers the possibility of making more complex and interesting nanoscale features by modulation of the applied dose and acceleration voltage, both of which control the scattering of electrons in the substrate (14, 15). Our studies on the effect of the accelerating voltage and applied charge on various surface-immobilized proteins have resulted in a novel method for the fabrication of nanoring structures that show a significant difference from dots regarding the formation of cell adhesion complexes.

The fabrication process is outlined in Figure 1. A silicon wafer surface was functionalized before coating with (3-aminopropyl)triethoxysilane (APTES), which induces subsequent protein adhesion. A solution of the first protein of interest is incubated with the APTES-coated surface before being rinsed, dried, and exposed to a focused electron beam. The substrate is then incubated with a second protein solution to complete the backfilling step. Staining with antibodies shows positioning of the proteins on the surface. Previously, we showed that electron beam irradiation does not change the surface topography but rather the surface functionality, as determined by phase-mode imaging with atomic force microscopy (AFM), which is sensitive to a chemical change in the protein on the surface (15).
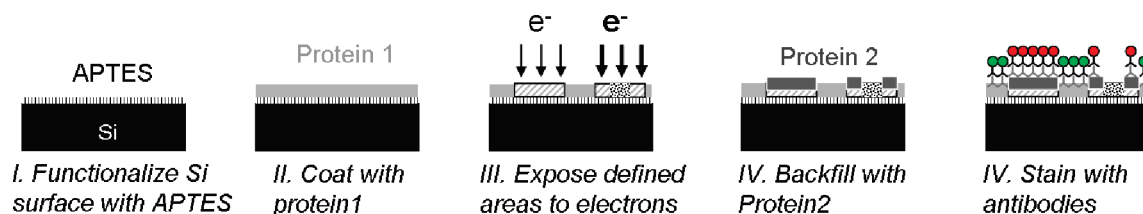
FIGURE 1. Fabrication process. An APTES-functionalized silicon wafer is coated with protein of interest (1). After electron beam exposure, the surface is incubated with the second protein of interest (2). Immunostaining can be performed for both proteins, revealing the surface pattern.
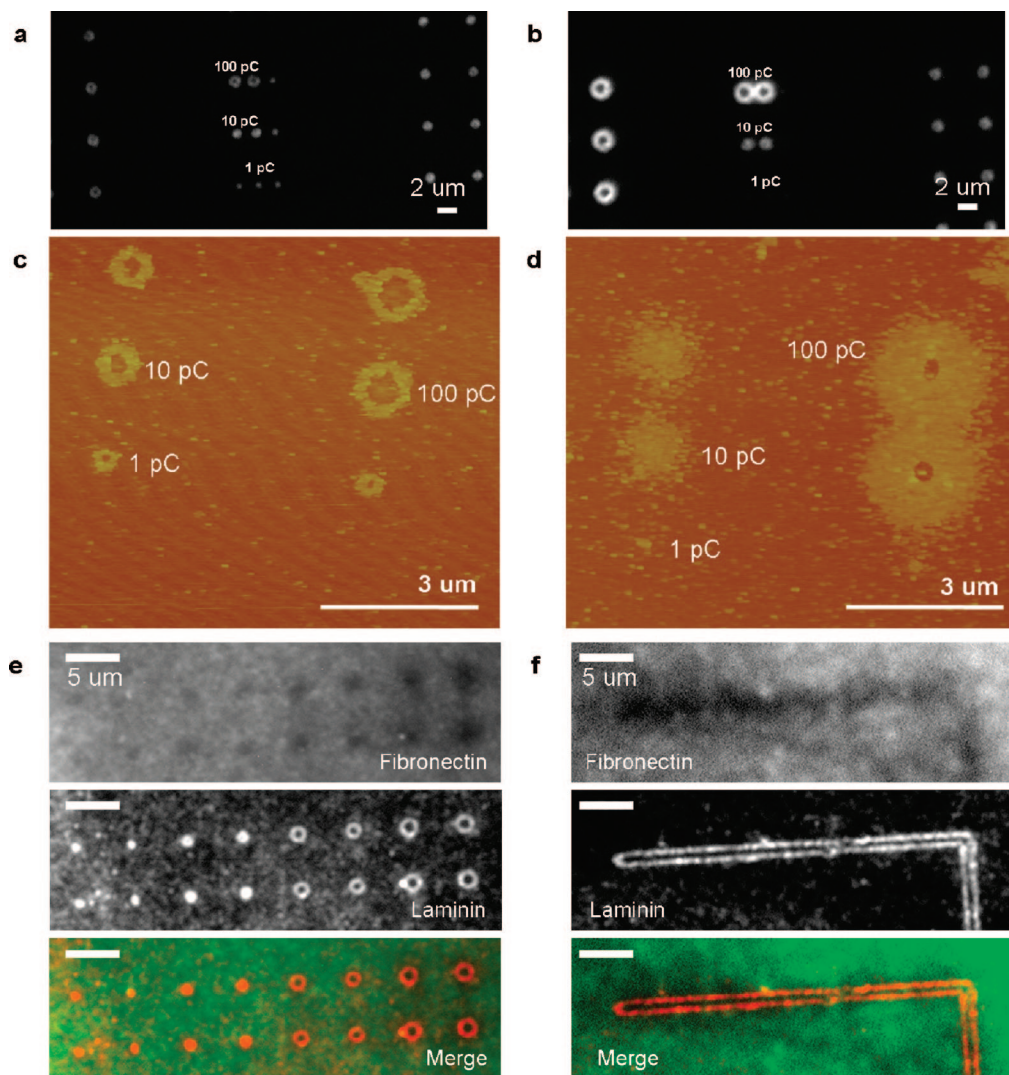

FIGURE 2. Various proteins can be patterned into nanodots and nanorings. (a–d) FN patterns on a K-Casein background stained with FN-specific antibodies. (a and b) Immunofluorescence images. (c and d) AFM images. (a and c) Patterning performed at 5 kV. (b and d) Patterning performed at 10 kV. (e) Laminin patterns on FN background stained with FN-specific (green) and laminin-specific (red) antibodies. The point exposure mode is used. (f) Same as part e, except using the line exposure mode.

In this work, we performed patterning with two different combinations of proteins. One combination consisted of the blocking protein, K-Casein, and a cell-adhesion-inducing protein, FN, and the other combination used two cell-adhesion-promoting proteins (FN and laminin). Figure 2a shows a substrate of K-Casein background with FN backfilled before being stained with FN-specific antibodies. Our previous work demonstrated that a threshold dose is required to cause the second protein in the pair to self-assemble and form a nanodot at the exposed site. We showed that the size

of the nanodot increases with the applied charge (15). Here we show that if the charge deposited by the electron beam is further increased, ring-shaped structures are produced when the second protein assembles on the surface. We interpret the formation of this ring as resulting from another, higher threshold dose, which when applied to the surface, inhibits binding of the second protein (Figure S1 in the Supporting Information).

At the accelerating voltages of 5 and 10 kV, the applied electron beam carrying a charge of 1 pC activated ring-

shaped and circular areas, respectively, for the adhesion of the second protein species (Figure 2). AFM images of rings patterned at 10 kV resolve that the ring area for FN adherence is larger than expected from fluorescence images. This difference is probably due to the diffraction effects of light microscopy, perhaps related to the orientations of the fluorophores conjugated to antibodies. Comparing two accelerating voltages, we show that the charge required for ring formation is higher at the accelerating voltage of 10 kV compared to 5 kV, indicating that the major surface modification is brought about by secondary backscattered electrons. The fact that the inner boundaries of the ring patterns are better defined than the outer boundaries at 10 kV suggests that forward-scattering electrons are important for patterning at higher doses.

The control of protein adhesion with the electron beam dose can be applied to a wide range of proteins. The method then allows for the creation of a two-component biofunctional template with one process sequence. A substrate coated with FN, exposed to the electron beam, and backfilled with laminin shows two distinct biofunctionalities when stained with both FN- and laminin-specific antibodies (Figure 2e,f). Here, we see the advantage of using proteins as active materials with the backfilling approach. FN exposed to a focused electron beam at low applied surface charge is amended so that laminin can bind to exposed areas. As the applied charge increases, the FN surface is modified in such a way so as to prevent laminin adhesion at the center of the exposed areas that are receiving the maximum charge. This dose-dependent change in the affinity for binding of the backfilled protein occurs not only for point exposures but also for line exposures (Figure 2f; area exposures are given in Figure S1 in the Supporting Information). Because the line is created by a sequence of point exposures, lines that receive a high applied charge per unit length will create double-lines when backfilled with the second protein. The double lines are connected at the start of the pattern because the applied dose dips below the threshold dose for binding inhibition at the each end of the line.

The nanopattern radii up to ∼1230 nm were plotted as a function of the applied dose. Assuming a Gaussian point spread function for the scattered electrons, we can fit our data as described previously (14) to determine the threshold doses and characteristic spreading radii for enabling and inhibiting protein binding. These are 132 pC/cm^2, 217 nm, for enabling and 2334 pC/cm^2, 134 nm, for inhibiting protein binding (backfilling) to a K-Casein-coated silicon surface at 5 kV accelerating voltage (Figure 3). For 10 kV, the corresponding values were 125 pC/cm^2, 557 nm, and 11 970 pC/cm^2, 76 nm. The doubling of the spreading radius for enabling protein binding from 5 to 10 kV is consistent with the picture that exposure of the protein is due to backscattered electrons. At higher accelerating voltage, the backscattered and secondary electrons have enough energy to break bonds in the protein, leaving behind a material that enables the binding of the backfilled protein species. In contrast to this, the decrease in the spreading radius for inhibiting
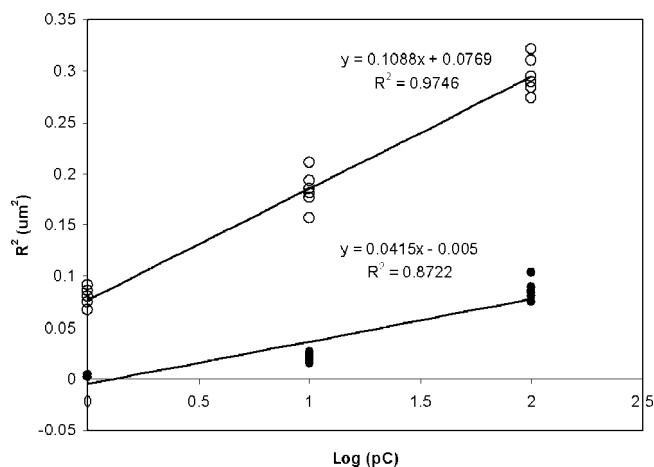

FIGURE 3. Accelerating voltage and applied charge which determine the shape and size of FN nanopatterns on the K-Casein background. The inner (●) and outer (○) radii of the FN patterns were measured using AFM images of antibody-stained K-Casein: FN substrates were patterned at 5 kV. The data are fit to a Gaussian distribution because of the stochastic nature of the fabrication and labeling processes.

protein binding when going from 5 to 10 kV and the large threshold doses required in each case suggest that forward-scattered electrons are responsible for the surface modification, which inhibits binding of the backfilled protein species.

To study the biofunctionality of the substrates with dot and ring features, we cultured endothelial cells on nanodot and nanoring patterns of FN on a K-Casein background (Figure 4). Previously, we have tested the ability of fibroblasts to form FAs on FN nanodots on a bovine serum albumin background (14, 15). K-Casein proved to be a better blocking protein, resulting in much less FN adhesion away from the exposed areas, as determined from immunofluorescence, AFM, and cell adhesion assays. Endothelial cells were cultured for ∼1 h on FN nanodots and nanorings with or without cycloheximide, which blocks de novo protein synthesis and helps to prevent obscuring of the surface FN pattern by endogenous FN staining. In both cases, cells adhered to surfaces and formed protrusions toward both the nanodots and nanorings, in a more pronounced manner on the nanoring patterns. To confirm FA complex formation on nanodots and nanorings, we stained for vinculin, a component of FAs. Cells on nanodots showed circle-shaped vinculin staining, while cells on nanorings exhibited more prominent and ring-shaped staining that reflected the underlying surface FN pattern.

We performed AFM imaging on cells grown on patterns after fixation, permeabilization, and immunofluorescence staining (Figure 5). The staining helps to improve the contrast in the AFM images because the antibody molecules introduce a height difference. The cellular protrusions and contacts on FN nanodots and nanorings are clearly seen in the AFM images. The AFM images show that cells make intermittent contacts with the surface, forming adhesions only on the dots and rings where FN is available, clearly showing the presence of space between the ventral surface of the cell and the substrate, in agreement with previous observations (16−18). When grown on nanodots, cells formed fibrillar, presumably cytoskeletal, structures origi-
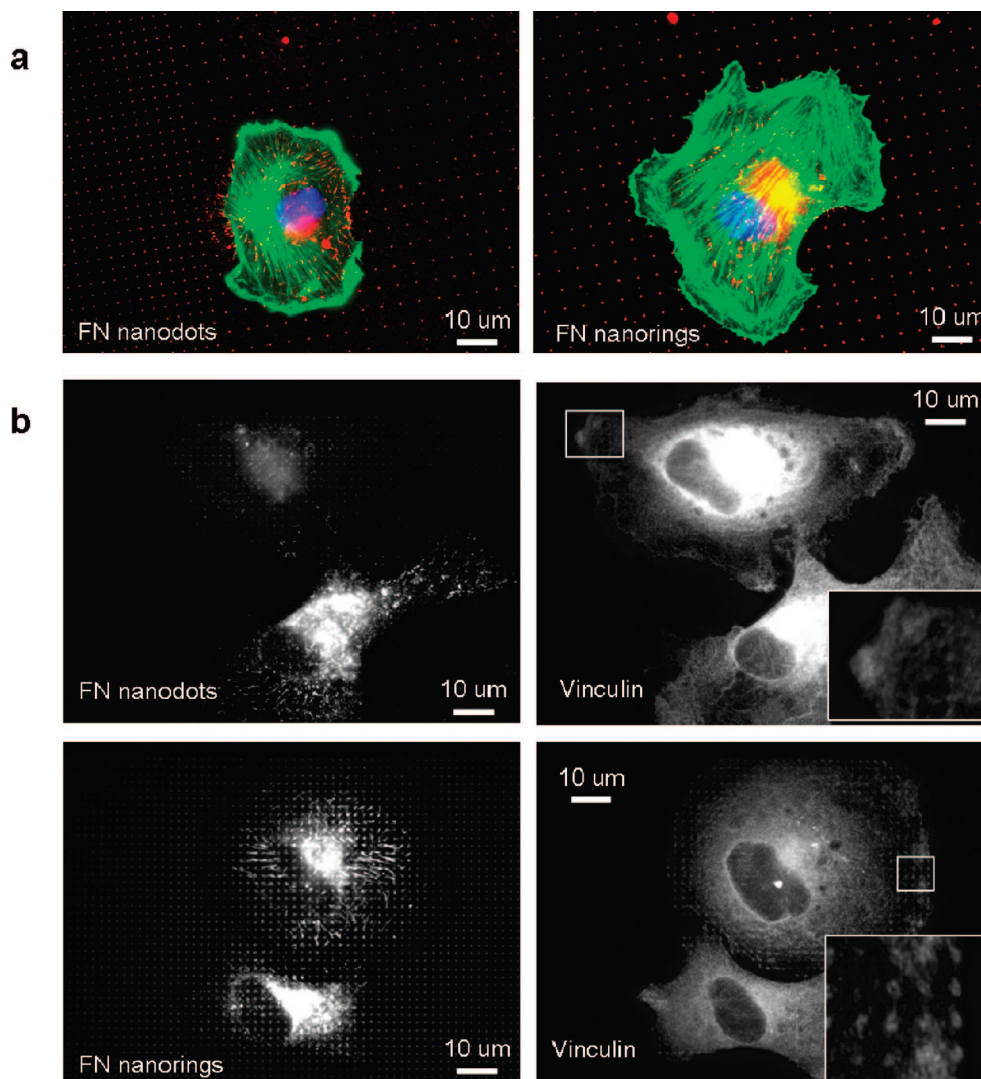
FIGURE 4. Endothelial cells adhere to nanopatterns of FN on a K-Casein background. (a) Cells contact FN nanopatterns and form stress fibers. Color coding: FN, red; actin, green; nucleus, blue. (b) Vinculin staining mirrors the FN patterns as dots or rings. Adhesions are stronger on nanorings, which present more FN molecules. Vinculin stainings reflect the underlying surface patterns of dots or rings (insets).

nating from the nanodot. On the other hand, cells on nanorings exhibited diverging fibril bundles extending from the nanorings. Both types of structures were 0.5−2 μm long. The bundle widths ranged from 0.4 to 1 μm. Because the fixed cells probed here are flattened onto the surface, we cannot exclude the possibility that the diverging fibril bundles are 2D projections of a 3D tubular structure. The nanodots in Figure 5 have an average radius of 153 nm, while the average nanoring inner and outer radii are 130 and 400 nm. The dimensions of FN patterns here are overestimated because of antibody staining and AFM tip broadening. FN immobilized to surfaces can have a radius of ~15 nm, depending on surface properties such as hydrophobicity (19, 20). Accordingly, there are ~100 and ~600 FN molecules per nanodot and nanoring, respectively. The higher number of FN molecules on nanorings is apparently resulting in increased vinculin recruitment (Figure 4). Here, we have investigated the minimal requirements for cell adhesion. How small can the pattern be for it to induce cell adhesion? When the nanodots were smaller than 100 nm, cells did not form pattern-specific adhesion. As we increased the applied

charge, we were able to increase the nanodot size and the cells responded with pattern-specific adhesion and robust actin staining at patterns larger than 1 μm (Figure S2 in the Supporting Information). We focused on smaller nanodots or nanorings here to determine a lower limit for adhesion to surface-presented molecules. Nanodots with a radius smaller than ~100 nm, which can contain ~40 FN molecules with a radius of 15 nm, were not able to induce pattern-specific cell adhesion. These data suggest that a minimum number of FN molecules immobilized on a surface is required to induce FA formation. It should be noted that accessibility of adhesion-inducing domains of FN can be limited after adsorption to the surface. If FN adopts an elongated form with an end-to-end distance of 100 nm, the number of available FN molecules per nanodot will be reduced to 4. Fibroblasts can have 5×10^5 integrins per cell (21). For a 25 μm × 50 um cell on a 5 μm spaced square lattice of nanodots or nanorings, ~5000 or ~30 000 FN molecules will be available, corresponding to 1% or 6% occupancy of integrins. A similar distribution can be expected for endothelial cells.
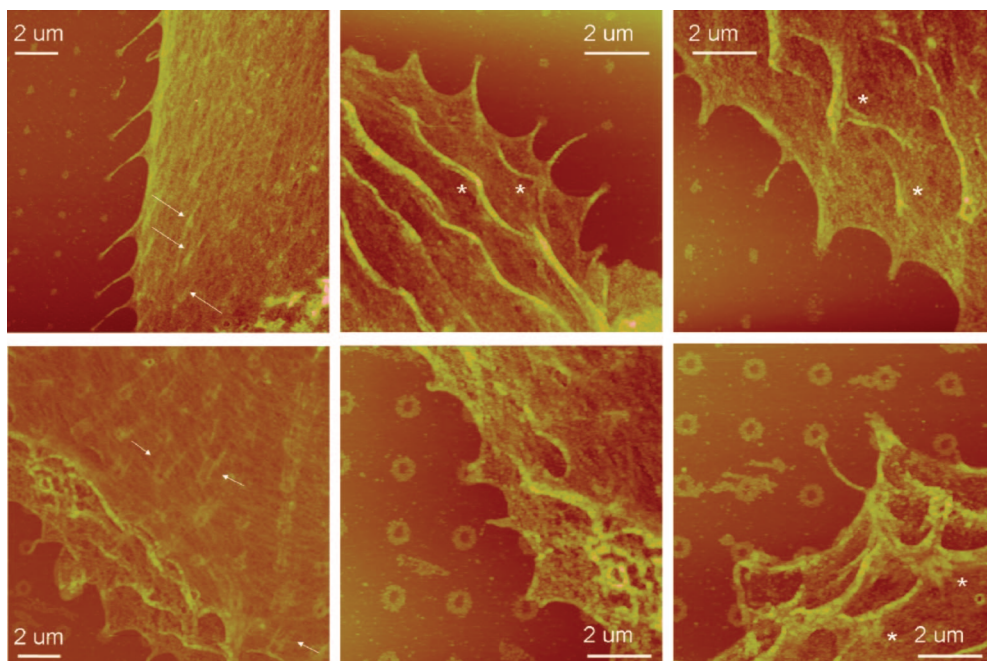
FIGURE 5. Cytoskeletal organization at FAs is modulated by surface patterns. Cells cultured with FN nanopatterns on a K-Casein background, fixed, permeabilized, and immunostained before imaging with AFM. Cells make intermittent contacts with the surface (*). Nanodots and nanorings induce fibrils (long arrows) and diverging fibril bundles (short arrows), respectively.

In summary, we have demonstrated that EBL can be employed to produce novel dot and ring, nanometer-scale surface patterns, using various proteins as active materials. The shape of nanometer-scale surface patterns can modulate FA complex organization and determine the organization of the adjoining cytoskeleton. By tailoring the size and distribution of FN surface patterns, we can establish specific requirements for cell adhesion. The methods demonstrated here offer the ability to rapidly fabricate nanometer-scale and arbitrary surface patterns with biofunctionality, highly suitable for basic cell biology studies as well as prototyping biotechnological applications.

EXPERIMENTAL SECTION

Protein Coating of Silicon Surfaces. Si(100) wafers of 500 μm thickness were cleaned with sonication in isopropyl alcohol and Milli-Q water followed by O_2 plasma treatment. The silicon surface was activated by immersion into a piranha solution (H_2SO_4/H_2O_2, 2:1, v/v) at room temperature for 15 min (*Toxic, fuming solution!*). The surfaces were extensively rinsed with Milli-Q water (3 times for 10 min each) on a rotatory shaker before incubation in a APTES solution (2−3%, Sigma) for 15−20 min. The APTES-treated surface was baked at 110 °C for 15−20 min. The proteins (Sigma), bovine serum albumin fraction V (10 mg/mL), K-Casein (1.25 mg/mL), fibronectin (FN; 0.1 mg/mL), and laminin (0.1 mg/mL) were dissolved in a universal buffer [150 mM NaCl, 5 mM Tris-HCl, 0.1% (w/v) NaN_3, pH 7.6] and filtered through 0.2 μm Acrodisc syringe filters with HT-Tuffryn membranes. The APTES-coated silicon surface was incubated with the first protein of interest for 2−3 h at room temperature, rinsed with Milli-Q water, and dried under nitrogen before electron beam exposure. Electron-beam-exposed surfaces were backfilled with the second protein of interest for 2−3 h at room temperature, rinsed with Milli-Q water, and dried under nitrogen. We have tested different FN concentrations and backfilling incubation times so that we do not overwrite the electron beam exposure pattern with excess protein adsorption. Using 0.1 mg/mL FN and room temperature incubation for 2−3 h resulted in an optimal contrast as determined by immunofluorescence. The electron-beam-exposed areas on K-Casein have a much higher affinity for the FN and are saturated at the end of the backfilling incubation.

EBL. A Raith 150 Turnkey system with a high-precision interferometric stage (Raith GmbH, Dortmund, Germany) was used to expose protein-coated silicon surfaces. The accelerating voltage was set to 5 or 10 kV at 30 μm aperture. Patterns were designed using *Raith 150* software in GDSII format.

The dose is controlled through accurate control of the time spent at each point, with a fixed and stable beam current. When we change the accelerating voltage from 5 to 10 kV, the current increases from ∼0.12 to ∼0.17 nA. To apply 1 pC at 5 kV, the time the focused electron beam spends on the designated coordinates is longer than the time for 10 kV and 1 pC. The resulting sizes and shapes of the surface protein patterns depend on the charge applied (time at a specific current) and the accelerating voltage, or electron energy, which effects the scattering radius of the electrons.

AFM. Patterned surfaces were inspected with a Multimode atomic force microscope with a J-scanner and a NanoScopeIV controller (Veeco Metrology Group, Digital Instruments, Santa Barbara, CA). Triangular cantilevers with sharp tips (nominal radius of curvature of 10 nm) and nominal spring constants of 0.03 N/m (MSCT-AUHW) were used for contact-mode imaging. Images were processed and analyzed with NanoScope Software v6.13r1.

Cell Culture. Human endothelial cells HUVEC-C (ATCC) were grown in a F12-K medium with 10% fetal bovine, heparin, and endothelial cell growth supplement at 37 °C and 5% CO_2. Cells were passaged 2−3 times per week with Trypsin-EDTA (0.25%). Cells were cultured on patterned surfaces for 1 h with or without cycloheximide (25 μg/mL). Cells were then fixed and permeabilized with paraformaldehyde (3.7%) and Triton X-100 (0.1%).

Immunofluorescence. The patterned substrates were stained with FN- or laminin-specific primary antibodies (Sigma, diluted 1:50−1:100), followed by TRITC- or FITC-conjugated antirabbit or antimouse antibodies produced in goat (Sigma, diluted 1:200−1:300).

Cells grown on patterned surfaces were stained for FN (Sigma, rabbit anti-FN, diluted 1:100; TRITC-conjugated goat antirabbit diluted 1:200), for actin filaments (Molecular Probes, Alexa Phalloidin 488), for vinculin (Sigma, FITC-conjugated mouse antivinculin 1:100; goat antimouse diluted 1:200), and for DNA (Sigma, Hoechst).

Samples were mounted using FluorSave (Calbiochem). Imaging was performed with a Nikon epifluorescence microscope with a 100X oil immersion objective, a 12-bit-cooled SPOT RT Monochrome CCD camera, and SPOT Advanced image acquisition software (Diagnostics Instruments, Sterling Heights, MI).

Supporting Information Available: Figures on thresholds that govern surface patterning and area exposures (Figure S1) and cell adhesion and surface patterns (Figure S2). This material is available free of charge via the Internet at http://pubs.acs.org.

REFERENCES AND NOTES

(1) Romer, L. H.; Birukov, K. G.; Garcia, J. G. N. *Circ. Res.* **2006**, *98*, 606.

(2) Chen, C. S.; Mrksich, M.; Huang, S.; Whitesides, G. M.; Ingber, D. E. *Science* **1997**, *276*, 1425.

(3) Thery, M.; Racine, V.; Pepin, A.; Piel, M.; Chen, Y.; Sibarita, J. B.; Bornens, M. *Nat. Cell Biol.* **2005**, *7*, 947.

(4) Christman, K. L.; Enriquez-Rios, V. D.; Maynard, H. D. *Soft Matter* **20006**, *2*, 928.

(5) Hoff, J. D.; Cheng, L. J.; Meyhofer, E.; Guo, L. J.; Hunt, A. J. *Nano Lett.* **2004**, *4*, 853.

(6) Falconnet, D.; Csucs, G.; Grandin, H. M.; Textor, M. *Biomaterials* **2006**, *27*, 3044.

(7) Harnett, C. K.; Satyalakshmi, K. M.; Craighead, H. G. *Langmuir* **2001**, *1*, 7–178.

(8) Kunzi, P. A.; Lussi, J.; Aeschimann, L.; Danuser, G.; Textor, M.; de Rooij, N. F.; Staufer, U. *Microelectron. Eng.* **2005**, *78*, 582.

(9) Kumagai, S.; Yoshii, S.; Yamada, K.; Fujiwara, I.; Matsukawa, N.; Yamashita, I. *J. Photopolym. Sci. Technol.* **2005**, *18*, 495.

(10) Rundqvist, J.; Hoh, J. H.; Haviland, D. B. *Langmuir* **2006**, *22*, 5100.

(11) Rundqvist, J.; Mendoza, B.; Werbin, J. L.; Heinz, W. F.; Lemmon, C.; Romer, L. H.; Haviland, D. B.; Hoh, J. H. *J. Am. Chem. Soc.* **2007**, *129*, 59.

(12) Cavalcanti-Adam, E. A.; Micoulet, A.; Blummel, J.; Auernheimer, J.; Kessler, H.; Spatz, J. P. *Eur. J. Cell Biol.* **2006**, *85*, 219.

(13) Alsberg, E.; Feinstein, E.; Joy, M. P.; Prentiss, M.; Ingber, D. E. *Tissue Eng.* **2006**, *12*, 3247.

(14) Pesen, D.; Heinz, W. F.; Werbin, J. L.; Hoh, J. H.; Haviland, D. B. *Soft Matter* **2007**, *3*, 1280.

(15) Pesen, D.; Erlandsson, A.; Ulfendahl, M.; Haviland, D. B. *Lab Chip* **2007**, *7*, 1603.

(16) Braun, D.; Fromherz, P. *Phys. Rev. Lett.* **1998**, *81*, 5241.

(17) Giebel, K. F.; Bechinger, C.; Herminghaus, S.; Riedel, M.; Leiderer, P.; Weiland, U.; Bastmeyer, M. *Biophys. J.* **1999**, *76*, 509.

(18) Kataoka, N.; Iwaki, K.; Hashimoto, K.; Mochizuki, S.; Ogasawara, Y.; Sato, M.; Tsujioka, K.; Kajiya, F. *Proc. Natl. Acad. Sci. U.S.A.* **2002**, *99*, 15638.

(19) Vallieres, K.; Chevallier, P.; Sarra-Bournett, C.; Turgeon, S.; Laroche, G. *Langmuir* **2007**, *23*, 9745.

(20) Bergkvist, M.; Carlsson, J.; Oscarsson, S. *J. Biomed. Mater. Res., Part A* **2003**, *64A*, 349.

(21) Akiyama, S. T.; Yamada, K. M. *J. Biol. Chem.* **1985**, *260*, 4492.

AM800264H